

Modelling and Simulation of the Effect of Air Damping on the Frequency and Quality factor of a CMOS-MEMS Resonator

J. O. Dennis¹, A. Y. Ahmed^{2,*}, M. H. Md. Khir² and A. A. S. Rabih²

¹ Department of Fundamental and Applied Sciences, Universiti Teknologi PETRONAS, Bandar Seri Iskandar, 31750 Tronoh, Perak, Malaysia

² Department of Electrical and Electronic Engineering, Universiti Teknologi PETRONAS, Bandar Seri Iskandar, 31750 Tronoh, Perak, Malaysia

Received: 23 May 2014, Revised: 22 Aug. 2014, Accepted: 24 Aug. 2014

Published online: 1 Mar. 2015

Abstract: This paper reports analytical modeling and finite element analysis (FEA) of the effect of two types of air damping (squeeze film and slide film damping) on resonance frequency and quality factor of a multi-layer CMOS-MEMS resonator designed for application as a mass sensitive gas sensor. The sensing principle is based on change in frequency or amplitude of the resonator due to adsorption/absorption of trace gases onto an active material to be deposited on the resonator membrane plate. The effect of air damping for mode 1 and mode 2 are investigated and the damping coefficient is found to increase from 0.922×10^{-6} Ns/m to 1.768×10^{-6} Ns/m for mode 1 and from 0.914×10^{-6} Ns/m to 1.708×10^{-6} Ns/m for mode 2 with increase in the overlap area of the fingers from $40 \mu\text{m}$ to $75 \mu\text{m}$, respectively. The quality factor (Q) of the CMOS-MEMS resonator is found to decrease with increasing damping coefficient for both modes of vibration while the frequency remained unaffected. Analytical and simulation results shows good agreement for damping coefficient (1.43 % and 1.22 %), resonant frequency (3.45 % and 4.4 %) and quality factor (2.27 % and 0.88 %) for mode 1 and 2, respectively.

Keywords: CMOS-MEMS resonator, quality factor, squeeze film damping, slide film damping

1 Introduction

MicroElectroMechanical Systems (MEMS) are devices that integrate mechanical elements such as sensors, actuators, and electrical and electronic components on a common silicon substrate. Other benefits of using MEMS technology include reduction in size, low power consumption and low cost through batch fabrication. The most common validation technique for MEMS devices before fabricating them is through finite element analysis (FEA) simulation. In MEMS gas detection structures, air damping (squeeze and slide film damping) [1,2] are the main sources of energy dissipation and they have a significant effect on the frequency and quality factor. In the fabrication of Complementary Metal-Oxide Semiconductor (CMOS) MEMS devices, two technological methods are used to release the device: front-side and back-side etching [3,4]. In the front-side etching, the substrate remains in close proximity to the

moving structure and therefore may significantly affect the damping in modes 1 and 2 depending on the gap between the moving structure and the substrate. While in backside etching the substrate is completely removed and will significantly reduce the air damping especially squeeze film damping in mode 2.

For some applications of CMOS-MEMS devices, the energy dissipated by squeeze and slide film damping must be reduced in order to maximize the motion of mechanical parts with limited energy supply and thereby improve sensitivity. Therefore, estimating the squeeze and slide film damping effect of these devices is an important step in their optimization. Currently, in order to optimize the effect of air damping (squeeze or slide film damping), the gap between the rotor, stator and substrate parts of the CMOS-MEMS structures has to be increased or alternatively holes/perforation have to be made on the resonating structures (plate) as reported by various

* Corresponding author e-mail: azez23101@gmail.com

papers [5,6,7]. Making holes in microstructures is effective in reducing the squeeze film damping effects due to horizontal air flow; however the air flow escaping through perforated holes brings new viscous resistance. Due to this fact, the conventional Reynolds formula for analysing squeeze-film effects of non-perforated planar structures is no longer applicable [8]. A lot of efforts have been focused on different ways to figure out and analyse the effect of squeeze film damping [2,9,10,11,12]. Within the assumption that air is incompressible, several reports offered analytical formulas and numerical evaluation to observe the squeeze-film damping. In addition to analytical investigation, several different techniques such as finite element methods have been utilized to determine squeeze-film damping [13,14].

In this paper we report on modeling of the mechanical behaviour of a CMOS-MEMS resonator etched from the backside in its first two modes of vibration that enables us to predict the effect of the two types of air damping, squeeze and slide film, on the resonance frequency and quality factor of the CMOS-MEMS resonator and validation of the results using FEA simulation.

2 Design of the CMOS-MEMS Resonator

The CMOS-MEMS resonator in this study is intended for use as a mass sensitive device for gas detection reported in details elsewhere [15,16,17]. In brief, the resonator is electrostatically actuated using comb-fingers and its motion detected using capacitive sensing. Figure (1-a) show the top view of the plate supported by four beams with each beam having two sections of different widths of $7\ \mu\text{m}$ and $19\ \mu\text{m}$ but same length of $240\ \mu\text{m}$ each. The rotor comb-fingers are attached to both the $400\ \mu\text{m} \times 400\ \mu\text{m}$ plate and to the thick $19\ \mu\text{m}$ beam (beam 2 in Figure (1-a)). All the comb fingers for either electrostatic actuation or sensing have width of $7\ \mu\text{m}$ and length of $80\ \mu\text{m}$. The device is intended for fabrication using $0.35\ \mu\text{m}$ CMOS process technology and post-CMOS micro-machining. The process technology consists of two poly, three metal layers, several dielectric layers and two vias. All metal layers are aluminum, silicon dioxide is used as the dielectric layer and tungsten is used as the vias. The overall thickness of the resonator plate is $20\ \mu\text{m}$ with $5\ \mu\text{m}$ made up of the CMOS layers and $15\ \mu\text{m}$ of single crystal silicon (SCS). Deep Reactive Ion Etching (DRIE) is used to etch the SCS substrate from the backside (which is initially about $350\ \mu\text{m}$) to leave a $15\ \mu\text{m}$ thick SCS layer underneath the CMOS layers to define the resonator structure. While Reactive Ion Etching (RIE) is used to etch silicon dioxide from the front side followed by front side DRIE to etch through the $15\ \mu\text{m}$ SCS substrate and release the resonator structure. The details of the fabrication and post-CMOS process are reported in [17]. Figure (1-b) shows the cross-sectional view across AA' of the structure to show the CMOS layers and the $15\ \mu\text{m}$ SCS substrate. Table 1 show the

standard material properties of all the CMOS layers which were used in the mathematical modeling and simulations, while Table 2 gives the dimensions of the various components of the device.

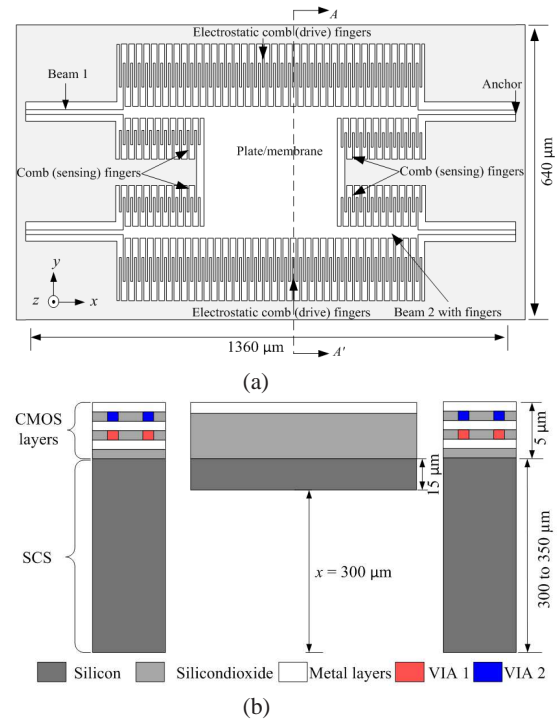


Fig. 1: Schematic of the (a) top view and (b) cross-section of the CMOS-MEMS resonator

Table 1: Material properties of the CMOS layers

Properties	Si	SiO_2	Al
Young's modulus (GPa)	130	72	70
Density (kg/m)	2300	2648	2700

Table 2: Dimensions of the CMOS-MEMS resonator

Parameter	Model symbol	Dimension (μm)
Device length		1360
Device width		640
Membrane area		400×400
Comb-finger length	l_{cf}	80
Comb-finger width	w_{cf}	7
Comb-finger thickness	t_{cf}	20
Comb-finger overlap area	l_o	40
Stator to rotor comb-finger gap	d	4
Length beam ₁	l_{b1}	240
Width beam ₁	w_{b1}	19
Length beam ₂	l_{b2}	240
Width beam ₂	w_{b2}	7

The theoretical concepts of the CMOS-MEMS resonator are developed using appropriate principles of electromechanical vibrations. The device is optimized for gas detection by modeling the effect of the two types of air damping on the resonant frequency and quality factor. Finally, the mathematically modeled device

characteristics are validated using FEA simulations. Figure (2 a and b) shows Field Emission Scanning Electron Microscope (FESEM) image from front side and backside of the successfully fabricated CMOS-MEMS resonator.

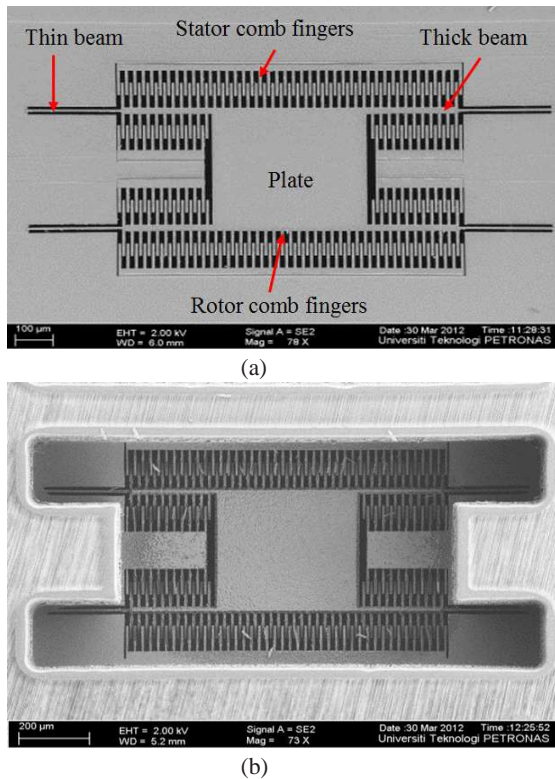


Fig. 2: FESEM image of the CMOS-MEMS resonator from (a) front side and (b) backside.

3 Theoretical Modeling and Simulation of the CMOS-MEMS Resonator

3.1 Analytical modeling

Alternating electrostatic driving actuation method is used to actuate the CMOS-MEMS resonator by using push-pull driving force. The electrostatic force F_{el} was generated by an alternating voltage ($V_{ac} \cos(\omega t)$) with a dc bias (V_{dc}) applied to the driving comb-fingers (upper and lower comb-fingers in Figure 1.a) using equation 1 [18,19].

$$F_{el} = \frac{4n\epsilon_0 h}{d} V_{dc} V_{ac} \quad (1)$$

where n is the number of fingers, ϵ_0 is the permittivity of the free space, h is the effective overlapping height between the rotor and stator fingers and d is the gap between the rotor and stator fingers.

The dynamic behavior of the system vibration can be described by second order differential equation for forced oscillations [20,21,22] given by equation (2) and (3) for

mode 1 (displacement in the y direction in Figure 1. a) and mode 2 (displacement in the z direction in Figure 1. a)

$$m_{total} \frac{d^2 y}{dt^2} + b_y \frac{dy}{dt} + k_y y = F \cos(\omega t) \quad (2)$$

$$m_{total} \frac{d^2 z}{dt^2} + b_z \frac{dz}{dt} + k_z z = F \cos(\omega t) \quad (3)$$

where m_{total} , b_y , b_z , k_y , k_z and F are the equivalent mass of the system, damping coefficient, spring constant and amplitude of the external driving force for mode 1 and mode 2, respectively. $\frac{d^2 y}{dt^2}$, $\frac{d^2 z}{dt^2}$, $\frac{dy}{dt}$, $\frac{dz}{dt}$, y and z are the acceleration, velocity and displacement of the mass, respectively. The resonator is modeled as mass-spring-damper system as depicted in Figure 3.

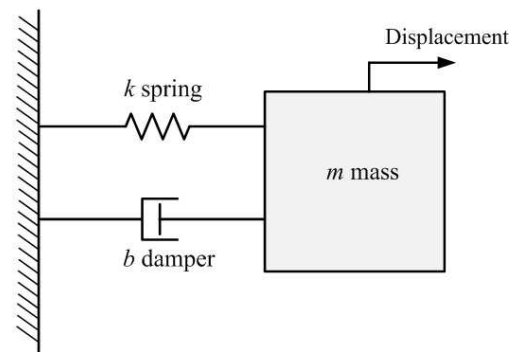


Fig. 3: Resonator model as a mass-spring-damper system.

The resonance frequency f_n of the CMOS-MEMS resonator depends on the spring constants of the beams and the dynamic mass of its movable parts (consisting of the plate, beams and comb-fingers) [23,24,25]. The spring constant is an important parameter which determines the characteristics of the device. Energy methods are used to derive analytic formulas for spring constant [26]. The overall spring constant k_y for mode 1 (in-plane oscillations in the y direction) and k_z for mode 2 (out of plane oscillations in the z direction putting $l_{b1}=l_{b2}=l$ and $l_{b1}=l_{b2}=l_b$) are given by

$$k_y = \lambda \frac{E_{av} t (w_{b1}^3 w_{b2}^3)}{l_b^3 (w_{b1}^3 + w_{b2}^3)} \quad (4)$$

$$k_z = \lambda \frac{E_{av} t^3 (w_{b1} w_{b2})}{l_b^3 (w_{b1} + w_{b2})} \quad (5)$$

where λ is determined using appropriate boundary conditions to be 3 and 1.03 for mode 1 and mode 2 , respectively, and E_{av} is average youngs modulus of the composite materials composing the beams. The average youngs modulus of the composite materials composing beam 1 and beam 2 is determined by [27,28]

$$E_{av} = \frac{(E_{Si} E_{SiO_2} E_{Al}) V_t}{E_{SiO_2} E_{Al} V_{Si} + E_{Si} E_{Al} V_{SiO_2} + E_{Si} E_{SiO_2} V_{Al}} \quad (6)$$

where E_{Si} , E_{SiO_2} , E_{Al} , V_{Si} , V_{SiO_2} , and V_{Al} are the youngs modulus and volume of the silicon, silicon dioxide, and aluminum, respectively, while $V_t = V_{Si} + V_{SiO_2} + V_{Al}$. The effective mass (m_{eff}) of beam 1 and beam 2 under bending moment [29,30] are obtained using

$$m_{effb1} = \frac{13}{35} \rho_{av} l_{b1} w_{b1} t \quad (7)$$

$$m_{effb2} = \frac{13}{35} \rho_{av} l_{b2} w_{b2} t \quad (8)$$

where ρ_{av} is the average density of the CMOS layers and is estimated by using equation (9)[27,28,31,32]

$$\rho_{av} = \frac{\rho_{Si} \times t_{Si} + \rho_{SiO_2} \times t_{SiO_2} + \rho_{Al} \times t_{Al}}{t_{Si} \times t_{SiO_2} \times t_{Al}} \quad (9)$$

where ρ_{Si} , ρ_{SiO_2} , ρ_{Al} , t_{Si} , t_{SiO_2} and t_{Al} are the densities and thicknesses of the silicon, silicon dioxide, and aluminium layers, respectively. The total mass (m_{total}) of the CMOS-MEMS resonator is the sum of the effective mass of beams, mass of plate (m_p) and mass of the n comb-fingers (nm_{cf}) [29] and is given by equation (10)

$$m_{total} = 4m_{effb1} + 4m_{effb2} + m_p + nm_{cf} = \rho_{av} t \alpha \quad (10)$$

where $\alpha = (\frac{32}{35} l_{b1} w_{b1} + \frac{52}{35} l_{b2} w_{b2} + l_p w_p + n l_{cf} w_{cf})$ and n is the total number of rotor comb-fingers on the resonator (on beam 2 and plate).

The damping ratio is defined as the ratio of the actual damping coefficient b to the critical damping coefficient b_c as in equation (11), and the critical damping coefficient is determined by equation (12).

$$\zeta = \frac{b}{b_c} \quad (11)$$

$$b_c = 2 \sqrt{km} \quad (12)$$

The damping coefficient has a significant effect on the physical behavior of a mechanically vibrating system. There are two types of damping effects for the two modes of vibration of the CMOS-MEMS resonators: slide and squeeze film damping [33,34]. Slide film damping occurs between the adjacent parallel walls of the rotor and stator parts of MEMS devices [35]. Squeeze film damping occurs when the rotor plate moves towards the stator plate or substrate [36,37,38].

Mode 1 in our device is affected by both the squeeze film damping resulting from the rotor finger tips and the adjacent stator wall and slide film damping due to motion of the adjacent parallel walls of the rotor and stator comb-fingers and also beam 2 and plate with the substrate (not shown in the figure) as shown in Figure 4. Mode 2 is also affected by both the squeeze film damping resulting from

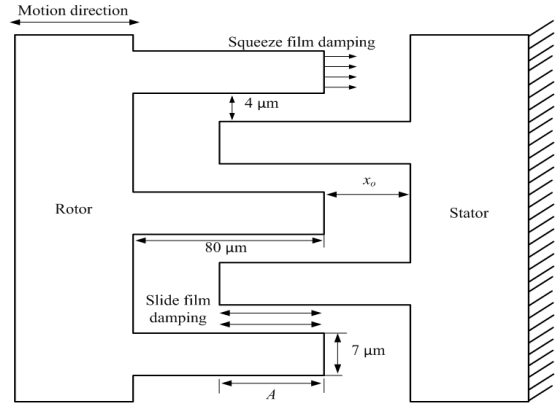


Fig. 4: Squeeze and slide film damping for mode 1

motion of the stator and rotor comb-fingers, beam 2 and plate toward the substrate and slide film damping between the stator and rotor comb-fingers.

The total damping coefficient for mode 1 and mode 2 are expressed as sum of squeeze and slide film damping as given by equation (13) and (14) for the two modes of vibration.

$$b_y = \eta \left[\frac{0.422n_1 t w_{cf}^3}{x_o^3} + \frac{2ntl_o}{d} + \frac{nl_{cf} w_{cf} + 4l_{b2} w_{b2} + l_p w_p}{x} \right] \quad (13)$$

$$b_z = \eta \left[\frac{0.422n_1 t w_{cf}^3 + 1.688l_{b2} w_{b2} + 0.422l_p^4}{x^3} + \frac{2ntl_o}{d} \right] \quad (14)$$

where η is the dynamic viscosity of air, nl is total number of stator and rotor fingers from one side, l_o is the comb-finger overlap area, x_o is the gap between the rotor comb-finger tips and stator wall and x is equal to 300 (back side etched SCS depth as shown in Figure 1.b). The resonance frequency under the effect of damping for mode 1 and mode 2 are determined by equation (15) and (16)

$$f_y = \frac{1}{\pi} \sqrt{\frac{k_y}{m_{total}} - \frac{b_y^2}{4m_{total}^2}} \quad (15)$$

$$f_z = \frac{1}{\pi} \sqrt{\frac{k_z}{m_{total}} - \frac{b_z^2}{4m_{total}^2}} \quad (16)$$

At resonance, the quality factor (Q) is expressed as [39].

$$Q = \frac{f_n}{f_1 - f_2} = \frac{\sqrt{m_{total}k}}{b} \quad (17)$$

where f_1 and f_2 are the frequencies at voltage gain of 0.707 or half power bandwidth and b is the damping coefficient. Q under the influence of damping for mode 1 and mode 2 are determined by equations (18) and (19) [19]

$$Q_y = \frac{\sqrt{m_{total}k_y}}{b_y} \quad (18)$$

$$Q_z = \frac{\sqrt{m_{total}k_z}}{b_z} \quad (19)$$

3.2 FEA Simulation

CoventorWare simulation software is used to design the device following $0.35 \mu\text{m}$ CMOS technology design rules and post-CMOS micromachining process to validate via FEA the performance characteristics of the CMOS-MEMS resonator. CoventorWare is a comprehensive virtual design environment for MEMS design and simulation tools that reduces design risk and manufacturing time and lowers development costs [40]. Material layers are constructed in a deposit and etch sequence that emulates the fabrication process to be used by the foundry. The virtual fabrication process in CoventorWare simulation software is defined in the process editor in the designer part of the software. The process editor supplies the information needed to construct the 3-D solid model of the resonator from the 2-D masks viewed in the layout editor. Figure 5 (a) shows the 3-D solid model of the CMOS-MEMS resonator from the front side and Figure 5 (b) shows the back-side of the resonator with thinner SCS ($15 \mu\text{m}$ thick) under the plate and beams achievable by etching. Fine tetrahedral mesh with $30 \mu\text{m}$ element size is used for all the layers of the resonator to obtain accurate simulation results.

In the simulation the damping MM solver is used to obtain the damping coefficient for mode 1 and mode 2 as the overlap area increases from $40 \mu\text{m}$ to $75 \mu\text{m}$. The simulation is performed in ambient pressure and temperature with frequency range of 10 kHz to 30 kHz, a frequency range that accommodates both the theoretically calculated resonance frequencies for mode 1 and mode 2. To obtain the simulated parameters of the device in the mechanical analysis, load force (the electrostatic) is calculated by using equation (1). However in the CoventorWare simulation environment, the driving load forces are given in terms of the pressure (force per unit area). Therefore the driving force that was calculated has to be converted to pressure for use in FEA simulation. The simulation of dynamic behaviour of the CMOS-MEMS resonator is performed using the modal harmonic analysis of the simulation software where the load force is a sinusoidal function of time to determine the vibrations of the two modes.

3.3 Comparison of Modeled and Simulation Results

Numerical solutions (Matlab) are used to investigate the effect of the squeeze and slide film damping on the resonance frequency and Q of the device. Figure (6) shows the theoretical effect on squeeze film damping of the distance of rotor comb-finger tips and the adjacent stator wall for mode 1, while Figure (7) shows theoretical and simulation results of the effect on slide film damping of comb-finger overlap area between the vertical side walls of the stator and rotor comb-fingers for mode 1 and mode 2 and shows good agreement.

It is theoretically observed that the squeeze film damping increases with decrease in gap distance between rotor

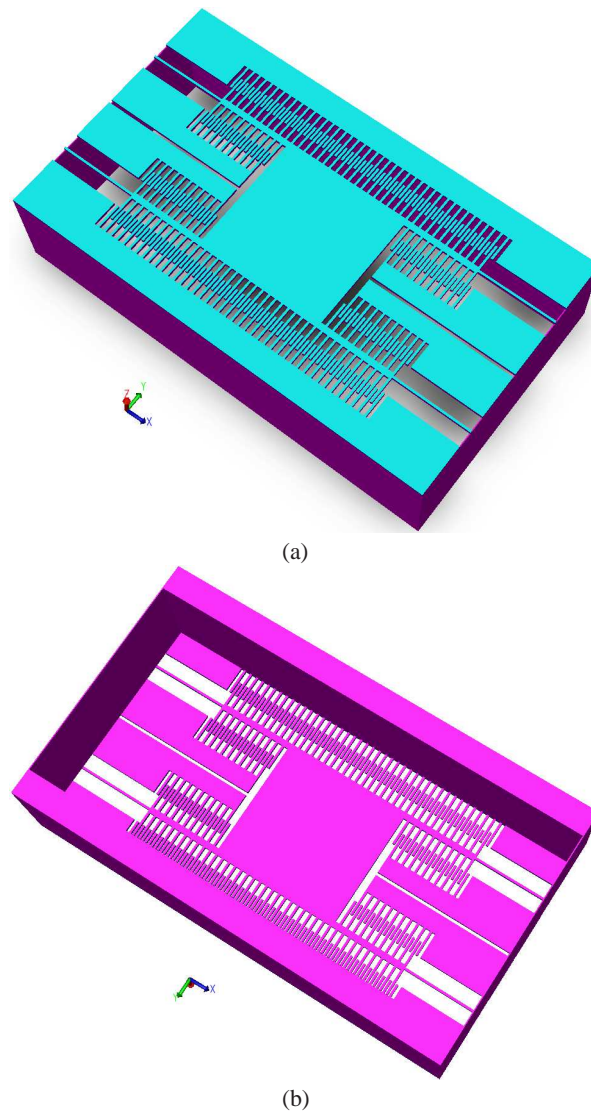


Fig. 5: 3-D solid model of the CMOS-MEMS resonator showing (a) top view and (b) back-side view

comb-finger tips and the adjacent stator wall for mode 1 while it remains constant ($7.2 \times 10^{-9} \text{Ns/m}$) for mode 2. However, the squeeze film damping is about two or three orders of magnitude lower than slide film damping and may therefore be neglected in the following analysis. The increase in slide film damping has a significant effect on the resonators Q , decreasing it from about 1436 to 749 for mode 1 and from 2124 to 1137 for mode 2, while having a negligible effect on the resonance frequency which remains unaffected at 18.38 kHz for mode 1 and 26.95 kHz for mode 2. Figures (8) shows typical simulation results of modal displacement at resonance frequency for (a) mode 1 with a resonance frequency of 17.75 kHz and mode 2 with 25.77 kHz at a damping coefficient of $0.922 \times 10^{-6} \text{Ns/m}$ and $0.914 \times 10^{-6} \text{Ns/m}$, respectively. Compared with the theoretically calculated values of 18.36 kHz and 26.95 using equations (15) and (16) for modes 1 and 2, respectively, the percentage error is

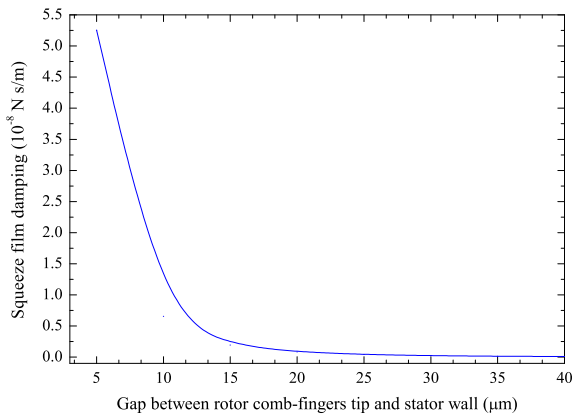


Fig. 6: Theoretical effect on squeeze film damping of gap of rotor comb-finger tips and the adjacent stator wall for mode 1.

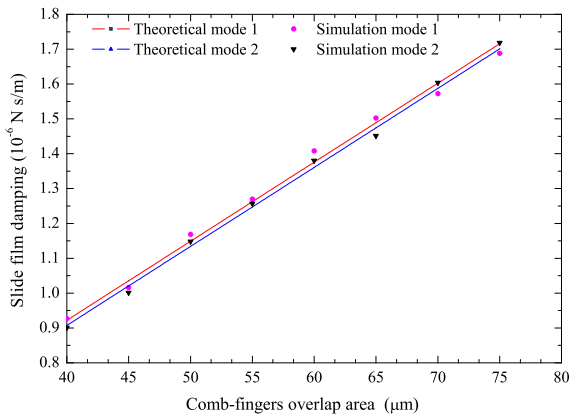


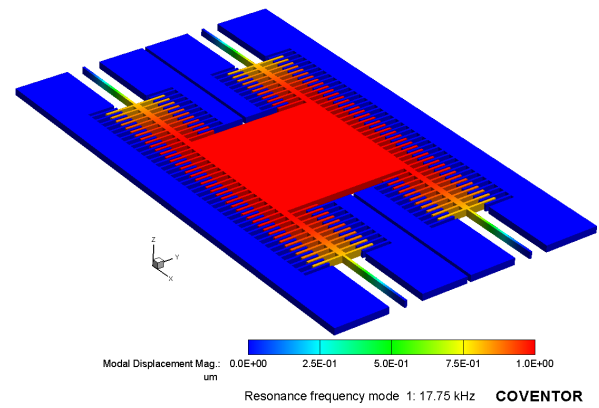
Fig. 7: Comparison of theoretical and simulation results of the effect on slide film damping of comb-finger overlap area between the vertical side walls of the stator and rotor comb-fingers for mode 1 and mode 2.

found to be 3.32 % and 4.38 %, respectively, showing a very good agreement.

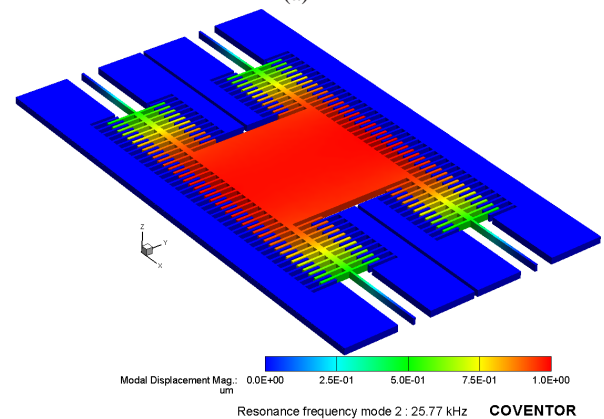
Figure (9) shows a comparison of theoretical and simulation results of the effect of damping on Q for (a) mode 1 and (b) mode 2. The agreement between modeled and simulated Q is 2.27 % and 0.88 % for mode 1 and 2, respectively. Results show that the quality factor decreases appreciably as the damping coefficient increases.

4 Conclusions

Mathematical modeling and FEA simulation of a CMOS-MEMS resonator has been presented. The effect of air damping on the resonant frequency and quality factor for mode 1 and mode 2 were investigated. The damping coefficient was found to increase from 0.922×10^{-6} Ns/m to 1.768×10^{-6}



(a)



(b)

Fig. 8: Typical FEA simulation of modal displacement at resonance frequency for mode 1 and (b) mode 2.

Ns/m for mode 1 and from 0.914×10^{-6} Ns/m to 1.708×10^{-6} Ns/m for mode 2 with increase in the overlap area of the fingers from 40 μm to 75 μm , respectively. As expected, the quality factor decreases with increasing damping coefficient, while the frequency of the CMOS-MEMS resonator remains unaffected at 18.38 kHz and 26.95 kHz for mode 1 and mode 2, respectively. Simulation results indicates that the resonant frequency for mode 1 mode 2 are 17.75 kHz and 25.77 kHz at a damping coefficient of 0.922×10^{-6} Ns/m and 0.914×10^{-6} Ns/m, respectively. The theoretical and simulation results show good agreement for damping coefficient (1.43 % and .22 %), resonant frequency (3.45 % and 4.4 %) and quality factor (2.27 % and 0.88 %) for mode 1 and mode 2, respectively.

Acknowledgment

The authors would like to thank Universiti Teknologi PETRONAS (UTP), Ministry of Science, Technology and Innovation (MOSTI) project No: 01-02-02-F0094 and Ministry of Higher Education (MOHE) under project No: 158-200-101 for financial and other support for the project.

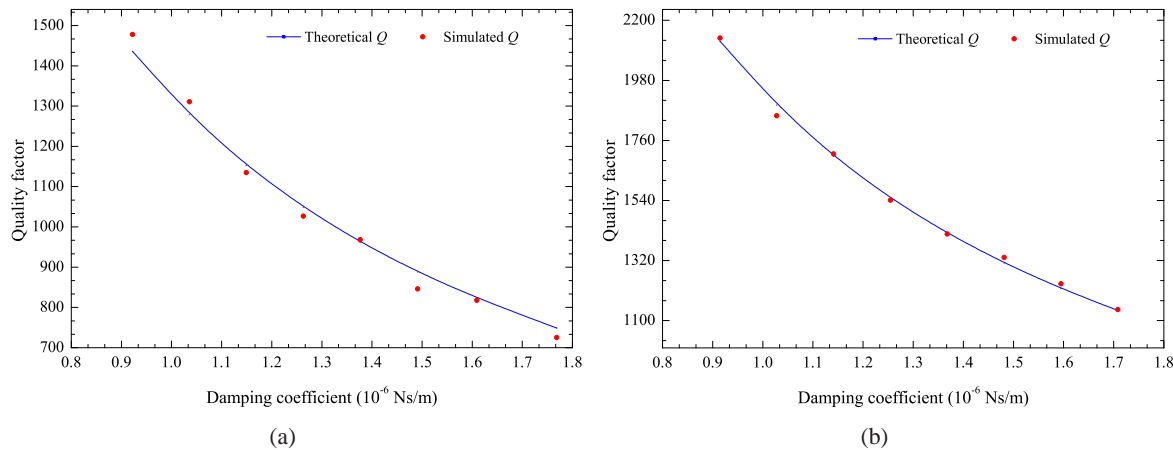


Fig. 9: Theoretical and simulation results of Q vs. damping coefficient for (a) mode 1 and (b) mode 2.

The authors are grateful to the anonymous referee for a careful checking of the details and for helpful comments that improved this paper.

References

- [1] H. Hosaka, K. Itao, and S. Kuroda, Damping characteristics of beam-shaped micro-oscillators, *Sensors and Actuators A: Physical*, **49**, 87-95 (1995).
- [2] M. Andrews, I. Harris, and G. Turner, A comparison of squeeze-film theory with measurements on a microstructure, *Sensors and Actuators A: Physical*, **36**, 79-87 (1993).
- [3] H. Qu, "Development of DRIE CMOS-MEMS Process and Integrated Accelerometers," Doctor Philosophy, University of Florida, Florida, (2006).
- [4] J. O. Dennis, F. Ahmad, and M. H. Khir, *CMOS Compatible Bulk Micromachining*, (2013).
- [5] P. Li, Y. Fang, and F. Xu, Analytical modeling of squeeze-film damping for perforated circular microplates, *Journal of Sound and Vibration*, **333**, 2688-2700 (2014).
- [6] M. Bao, H. Yang, Y. Sun, and Y. Wang, Squeeze-film air damping of thick hole-plate, *Sensors and Actuators A: Physical*, **108**, 212-217 (2003).
- [7] C. Li and M. H. Miller, Optimization Strategy for Resonant Mass Sensor Design in the Presence of Squeeze Film Damping, *Micromachines*, **1**, 112-128 (2010).
- [8] C. Feng, Y.-P. Zhao, and D. Q. Liu, Squeeze-film effects in MEMS devices with perforated plates for small amplitude vibration, *Microsystem Technologies*, **13**, 625-633 (2007).
- [9] P. Belardinelli, M. Brocchini, L. Demeio, and S. Lenci, Dynamical characteristics of an electrically actuated microbeam under the effects of squeeze-film and thermoelastic damping, *International Journal of Engineering Science*, **69**, 16-32 (2013).
- [10] H. Moeinfard and M. Taghi Ahmadian, The influence of vertical deflection of the supports in modeling squeeze film damping in torsional micromirrors, *Microelectronics Journal*, **43**, 530-536 (2012).
- [11] H. Sumali, Squeeze-film damping in the free molecular regime: model validation and measurement on a MEMS, *Journal of Micromechanics and Microengineering*, **17**, 22312240 (2007).
- [12] J. B. Starr, Squeeze-film damping in solid-state accelerometers, in *Solid-State Sensor and Actuator Workshop*, 1990. 4th Technical Digest., IEEE, 1990, pp. 44-47.
- [13] G. Schrag and G. Wachutka, Accurate system-level damping model for highly perforated micromechanical devices, *Sensors and Actuators A: Physical*, **111**, 222-228 (2004).
- [14] D. Yan and A. Lal, The squeeze film damping effect of perforated microscanners: modeling and characterization, *Smart Materials and Structures*, **15**, 480-484 (2006).
- [15] A. Y. Ahmed, J. O. Dennis, M. H. M. Khir, and M. N. M. Saad, Finite element analysis of a mass-sensitive CMOS-MEMS resonator using CoventorWare simulation software, in *4th International Conference on Intelligent and Advanced Systems (ICIAS)*, 2012, pp. 780-783.
- [16] A. Y. Ahmed, J. O. Dennis, M. H. M. Khir, and M. N. Mohamad Saad, "Simulation and modeling the effect of temperature on resonant frequency of a CMOS-MEMS resonator," *American Institute of Physics (AIP) Conference Proceedings*, vol. 1482, pp. 32-36, 2012.
- [17] A. Y. Ahmed, J. O. Dennis, M. H. Md Khir, M. N. Mohamad Saad and M. R. Buyong, Design, Simulation and Fabrication of a Mass Sensitive CMOS-MEMS Resonator, *Sensors and Transducers Journal*, vol. 17, pp. 40-49, 2012.
- [18] M. Bao and S. Middelhoek, *Micro Mechanical Transducers: Pressure Sensors, Accelerometers and Gyroscopes*: Elsevier Science, (2000).
- [19] S. Bedair, "Sub-nanogram Mass Loading CMOS-MEMS Cantilever Resonator Oscillators for Gas Detection," Doctor of Philosophy, Electrical and Computer Engineering, Carnegie Mellon University, (2008).
- [20] W. Weaver, S. P. Timoshenko, and D. H. Young, *Vibration Problems in Engineering*. New York: John Wiley and Sons, 1990.
- [21] C. W. de Silva, *Vibration: Fundamentals and Practice*, Second Edition: Taylor and Francis, 1999.

- [22] C. Acar and A. M. Shkel, MEMS vibratory gyroscopes: structural approaches to improve robustness: Springer, 2009.
- [23] Ying-Chung Li, Meng-Han Ho, Shi-Jie Hung, Meng-Huei Chen and Michael S-C Lu, CMOS micromachined capacitive cantilevers for mass sensing, *Journal of Micromechanics and Microengineering*, **16**, 2659-2665 (2006).
- [24] B. Ilic, D. Czaplewski, M. Zalalutdinov, H. G. Craighead, P. Neuzil, C. Campagnolo, et al., Single cell detection with micromechanical oscillators, *Journal of Vacuum Science and Technology B: Microelectronics and Nanometer Structures*, **19**, 2825-2828 (2001).
- [25] G Abadal, Z J Davis, B Helbo, X Borris, R Ruiz, A Boisen, F Campabadal, J Esteve, E Figueras, F Prez-Murano and N Barniol, Electromechanical model of a resonating nano-cantilever-based sensor for high-resolution and high-sensitivity mass detection, *Nanotechnology*, **12**, 100-104 (2001).
- [26] G. K. Fedder, Simulation of Microelectromechanical Systems, Doctor of Philosophy, Department of Engineering-Electrical Engineering and Computer Sciences, University of California at Berkeley, Berkeley, 1994.
- [27] R. M. Jones, *Mechanics of Composite Materials*: Hemisphere Publishing Corp, New York, 1975.
- [28] J. M. Berthelot, *Composite Materials: Mechanical Behavior and Structural Analysis*, Springer, Verlag, 1999.
- [29] W. Wai-Chi, A. A. Azid and B. Y. Majlis Formulation of stiffness constant and effective mass for a folded beam, *Archives of Mechanics*, **62**, 405-418 (2010).
- [30] Wai Chi Wong, Ishak Abdul Azid and Burhanuddin Yeop Majlis, Theoretical Analysis of Stiffness Constant and Effective Mass for a Round-Folded Beam in MEMS Accelerometer, *Journal of Mechanical Engineering*, **57**, 517-525 (2011).
- [31] D. Lange, C. Hagleitner, O. Brand, and H. Baltes, CMOS resonant beam gas sensing system with on-chip self excitation, in *Micro Electro Mechanical Systems, 2001. MEMS 2001. The 14th IEEE International Conference on*, 2001, pp. 547-552.
- [32] D. Lange, O. Brand, and H. Baltes, *CMOS Cantilever Sensor Systems: Atomic-Force Microscopy and Gas Sensing Applications*: Springer, 2002.
- [33] R. I. Shakoor, Design, Fabrication and Characterization of Metalmumps Based MEMS Gyroscopes, Doctor of Philosophy, chemical and Materials Engineering, Pakistan Institute of Engineering and Applied Sciences, 2010.
- [34] L. A. Rocha, Dynamics and Nonlinearities of the Electro-Mechanical Coupling in Inertial MEMS, Doctor of Philosophy, Electrical Engineering, Mathematics and Computer Science, Delft University of Technology, 2005.
- [35] T. Veijola and M. Turowski, Compact damping models for laterally moving microstructures with gas-rarefaction effects, *Journal of Microelectromechanical Systems*, **10**, 263-273 (2001).
- [36] M. J. Novack, Design and fabrication of a thin film micromachined accelerometer, Master of Science in Mechanical Engineering Department of Mechanical Engineering Massachusetts Institute of Technology, Massachusetts Institute of Technology, 1992.
- [37] K. Eung-Sam, C. Young-Ho, and K. Moon-Uhn, Effect of holes and edges on the squeeze film damping of perforated micromechanical structures, in *Micro Electro Mechanical Systems, 1999. MEMS '99. Twelfth IEEE International Conference on*, 1999, pp. 296-301.
- [38] N.-C. Tsai, C.-Y. Sue, and C.-C. Lin, Design and dynamics of an innovative micro gyroscope against coupling effects, *Microsystem Technologies*, **14**, 295-306 (2008).
- [39] T. Veijola, H. Kuisma, J. Lahdenper, and T. Ryhnen, Equivalent-circuit model of the squeezed gas film in a silicon accelerometer, *Sensors and Actuators A: Physical*, **48**, 239-248 (1995).
- [40] <http://www.coventor.com/products/coventorware/>.



J. O. Dennis obtained Bachelor of Education Degree in Physics and Mathematics from University of Juba, South Sudan in 1982, Masters of education from university of Khartoum, Sudan in 1987 and a PhD degree in Applied Physics from Universiti Teknologi Malaysia, Malaysia in 2001. He is currently

an Associate Professor in the Department of Fundamental and Applied Sciences, Universiti Teknologi PETRONAS, Malaysia, since 2011. From 2003 to 2011 he served as Senior Lecturer in the Department of Electrical and Electronic Engineering, Universiti Teknologi PETRONAS, Malaysia. His research interests include development of MEMS/NEMS devices for sensing applications.



A. Y. Ahmed was born in Sudan in 1980. He received his B.Sc in Electronic Engineering from University of Gezira, Sudan, in 2006, and M.Sc in Electrical and Electronics Engineering from Universiti Teknologi PETRONAS, Malaysia, in 2009. Currently, he is pursuing his PhD in Electrical

and Electronic Engineering at Universiti Teknologi PETRONAS (UTP), Malaysia. His research area is MEMS device design and fabrication based on CMOS-MEMS technologies.



M. H. Md. Khir received his B.Eng. degree in Electrical and Electronic Engineering from Universiti Teknologi MARA, Malaysia, in 1999, M.Sc in Computer and System Engineering from Rensselaer Polytechnic Institute, New York, USA, in 2001, and PhD degree in systems engineering from

Oakland University, MI, USA, in 2010. Since 2002, he has been with Universiti Teknologi PETRONAS, Malaysia, where he is currently serving as a Senior Lecturer in Electrical and Electronic Engineering Department. His research interests include MEMS sensors/actuators design and fabrication based on CMOS and MUMPS technologies.



A. A. S. Rabih was born in Sudan in 1983. He received his B.Sc. in electronic engineering (medical instrumentation), University of Gezira, Sudan, in 2008, and his M.Sc. in electrical and electronics engineering, Universiti Teknologi PETRONAS, Malaysia, in 2012. He is currently pursuing his PhD

in electrical and electronics engineering, Universiti Teknologi PETRONAS. His area of interest is Biomedical MEMS.